View metadata, citation and similar papers at core.ac.uk

brought to you by CORE

provided by Arrow@dit

Technological University Dublin

ARROW@TU Dublin

Articles

NanoLab

2017

Label-Free, High Content Screening Using Raman Microspectroscopy: The Toxicological Response of Different Cell Lines to Amine-Modified Polystyrene Nanoparticles

Esen Efeoglu
Technological University Dublin, esen.efeoglu@tudublin.ie

Alan Casey
Technological University Dublin, alan.casey@tudublin.ie

Hugh J. Byrne
Technological University Dublin, hugh.byrne@tudublin.ie

Marcus A. Maher
Technological University Dublin, Marcus.Maher@mydit.ie

Follow this and additional works at: https://arrow.tudublin.ie/nanolart

 Part of the Medicine and Health Sciences Commons

Recommended Citation

Efeoglu, E., Casey, A. & Maher, M. (2017). Label-free, high content screening using Raman microspectroscopy: the toxicological response of different cell lines to amine-modified polystyrene nanoparticles. *The Analyst*, August 2017. doi:10.1039/c7an00461c

This Article is brought to you for free and open access by the NanoLab at ARROW@TU Dublin. It has been accepted for inclusion in Articles by an authorized administrator of ARROW@TU Dublin. For more information, please contact yvonne.desmond@tudublin.ie, arrow.admin@tudublin.ie, brian.widdis@tudublin.ie.

This work is licensed under a Creative Commons Attribution-Noncommercial-Share Alike 3.0 License

Analyst

PAPER

View Article Online
View Journal

Published on 08 August 2017. Downloaded by Dublin Institute of Technology on 04/09/2017 12:27:54.

Check for updates

Cite this: DOI: 10.1039/c7an00461c

Label-free, high content screening using Raman microspectroscopy: the toxicological response of different cell lines to amine-modified polystyrene nanoparticles (PS-NH_2)†

Esen Efeoglu, *[a,b] Marcus A. Maher, [b] Alan Casey [b] and Hugh J. Byrne [b]

Nanotoxicology has become an established area of science due to growing concerns over the production and potential use of nanomaterials in a wide-range of areas from pharmaceutics to nanomedicine. Although different cytotoxicity assays have been developed and are widely used to determine the toxicity of nanomaterials, the production of multi-parametric information in a rapid and non-invasive way is still challenging, when the amount and diversity of physicochemical properties of nanomaterials are considered. High content screening can provide such analysis, but is often prohibitive in terms of capital and recurrent costs in academic environments. As a label-free technique, the applicability of Raman microspectroscopy for the analysis of cells, tissues and bodily fluids has been extensively demonstrated. The multi-parametric information in the fingerprint region has also been used for the determination of nanoparticle localisation and toxicity. In this study, the applicability of Raman microspectroscopy as a 'high content nanotoxicological screening technique' is demonstrated, with the aid of multivariate analysis, on non-cancerous (immortalized human bronchial epithelium) and cancerous cell-lines (human lung carcinoma and human lung epidermoid cells). Aminated polystyrene nanoparticles are chosen as model nanoparticles due to their well-established toxic properties and cells were exposed to the nanoparticles for periods from 24–72 hours. Spectral markers of cellular responses such as oxidative stress, cytoplasmic RNA aberrations and liposomal rupture are identified and cell-line dependent systematic variations in these spectral markers, as a function of the exposure time, are observed using Raman microspectroscopy, and are correlated with cellular assays and imaging techniques.

Received 16th March 2017,
Accepted 4th August 2017

DOI: 10.1039/c7an00461c

rsc.li/analyst

Introduction

The ease of interaction of nanomaterials with biological molecules and living systems can be utilized to design novel nanoparticles for gene and drug delivery, personalised medicine, diagnosis as well as imaging technologies.[1–4] Conversely, the physicochemical properties which give rise to this interaction and the high reactivity with biological systems can make them potentially toxic to humans.[5,6] When the amount and physicochemical diversity of naturally occurring and manufactured nanomaterials are considered, determination of toxic properties, possible adverse health effects and mechanism of action in a rapid, *in vitro* and multi-parametric fashion with a single assay carries significant importance to take full advantage from nanomaterials in a wide range of application areas. Various biological assays and imaging technologies have been introduced for the determination of cell–nanoparticle interactions, monitoring of nanoparticle uptake and localisation. The commercially available and well established cytotoxicity assays, Alamar Blue (AB), 3-(4,5-dimethylthiazol-2-yl)-2,5-diphenyltetrazolium bromide (MTT) and neutral red (NR), are nanotoxicological assessments recommended by the Organisation for Economic Co-operation and Development (OECD) for the determination of the nanoparticle toxicity.[7] However, the established techniques have remained limited due to the time needed for each experiment, requirement of multiple-labels and/or their invasive nature.

Over the last decade, High Content Analysis/Screening (HCA/HCS), which can be described as automated imaging and analysis of 'phenotypic assay endpoints' for the evaluation of multiple information sources regarding cell morphology, biochemical parameters in cells, tissue-level toxicity, as well as animal disease models, has brought a new perspective to, for

[a]School of Physics, Dublin Institute of Technology, Kevin Street, Dublin 2, Ireland. E-mail: esen.efeoglu@mydit.ie
[b]FOCAS Research Institute, Dublin Institute of Technology, Kevin Street, Dublin 2, Ireland

†Electronic supplementary information (ESI) available. See DOI: 10.1039/c7an00461c

Published on 08 August 2017. Downloaded by Dublin Institute of Technology on 04/09/2017 12:27:54.

example, drug discovery and academic research.[8–10] HCA has been used to replace cellular assays for cell signalling,[9,11,12] neurobiology,[13,14] *in vitro* toxicology,[10,15,16] cell physiology[17,18] and many other applications due to its speed, sensitivity and multifaceted data which provide advantages over conventional cellular assays. However, this technology still remains challenging because of the cost, problems in data management, development of application based models and lack of common standards.[8]

The applicability of Raman microspectroscopy to the investigation of biological systems has been demonstrated previously for tissues, cells, body fluids and also drug and nanoparticle screening.[19–26] The power of the Raman microspectroscopy to differentiate cellular regions such as nucleus, nucleolus and cytoplasm along with the localisation of nanoparticles has been shown by Dorney *et al.*[26] The localisation of the carboxyl modified-polystyrene nanoparticles (PS-COOH) at certain time points has been also demonstrated using Raman microspectroscopy and spectral biomarkers corresponding to cellular compartments such as endosomes, lysosomes and endoplasmic reticulum have been identified.[22] The correlation of Raman signatures with cytotoxicity assays for carbon nanotubes was demonstrated by Knief *et al.*[27] The importance of the combination of multivariate analysis techniques to extract information from Raman data sets regarding nanoparticle localisation in cellular regions has been demonstrated by Keating *et al.*[28] The ability of Raman microspectroscopy to determine spectral markers of the dose and time dependent cellular responses and the corresponding changes in biochemical constituents of the cells upon exposure to aminated polystyrene (PS-NH_2) nanoparticles has been also studied.[21]

Hereby, this study focuses on validation of the technique of Raman microspectroscopy as a label free, 'high content nanotoxicological screening' method in cancerous and non-cancerous cell lines based on spectral markers of cellular responses triggered by nanoparticle uptake. For this purpose, a non-cancerous, immortalized human bronchial epithelium cell line (BEAS-2B), and cancerous cell lines, human lung carcinoma (A549) and human lung epidermoid (Calu-1), are used, as they act as models for human exposure by inhalation. Aminated polystyrene nanoparticles (PS-NH_2) were chosen as model nanoparticles due to their extensively-studied toxic properties.[15,29–33] The toxic forms of the polystyrene nanoparticles (PS), *e.g.* PS-NH_2, have previously been demonstrated to result in ROS formation and oxidative stress upon exposure which triggers apoptosis by the release of inflammatory factors.[15,31,32,34] In this study, the effects of the PS-NH_2 on the cancerous and non-cancerous cell lines were evaluated by using the commercially available and well-established toxicity assays AB and MTT from 24 to 72 h for each cell line. Raman microspectroscopic studies were carried out at sublethal doses in order to observe the progressive evolution of the spectroscopic signatures of the toxicity in the fingerprint region for BEAS-2B, A549 and Calu-1 cells. Cells were exposed to PS-NH_2 from 24 to 72 h and corresponding controls for each cell line were prepared for comparison with the exposed cells. Raman spectra were acquired from the cytoplasm of the exposed and control cells and unsupervised principal component analysis (PCA) was used to evaluate changes upon PS-NH_2 exposure. Predicted toxic events based on Raman microspectroscopy such as oxidative stress and lysosomal damage were determined by using the 6-carboxy-2′,7′-dichlorodihydrofluorescein diacetate (carboxy-H_2DCFDA) dye and lysosensor, respectively and results were correlated with the Raman spectral markers.

Materials and methods

Nanoparticles and preparation of PS-NH_2 solutions

Commercially available, 100 nm amine-modified and fluorescently labelled polystyrene nanoparticles (PS-NH_2) were purchased from Sigma-Aldrich (L9904) and used throughout the study. The calculation of the stock concentration was made by using the manufacturer's instructions. Excitation and emission spectra are supplied by Sigma-Aldrich and have maxima at 481/644 nm, respectively.

PS-NH_2 working solutions were prepared by dispersing nanoparticles directly into the pre-heated (37 °C), 10% foetal bovine serum (FBS) and 2 mM L-glutamine supplemented in Dulbecco's Modified Eagle's Medium Nutrient Mixture F-12 HAM (DMEM-F12) or Roswell Park Memorial Institute (RPMI-1640) Medium, depending on the cell line. Initial stock concentration was calculated as 2.05 mM and working concentrations were freshly prepared prior to exposure. More information about working solutions and concentrations is supplied in the relevant sections of the following.

Reagents

For cytotoxicity evaluation of 100 nm PS-NH_2, 3-(4,5-dimethylthiazol-2-yl)-2,5-diphenyltetrazolium bromide (MTT) and Alamar Blue (AB) assays were purchased from Sigma Aldrich Ltd (Dublin, Ireland) and Biosource (UK), respectively. For the determination of reactive oxygen species (ROS), 6-carboxy-2′,7′-dichlorodihydrofluorescein diacetate (carboxy-H_2DCFDA) was purchased from Invitrogen (Ireland). In order to observe lysosomal activity and aberrations in intracellular pH, Lysosensor™ green DND-189 (L7535) was purchased from Life Technologies, Ireland.

Cell culture

Toxicological effects of 100 nm PS-NH_2 on cancerous and non-cancerous cell lines were evaluated. BEAS-2B (ATCC® CRL-9609™), a normal immortalized human bronchial epithelium cell line, was used as a model non-cancerous cell line, whereas A549 (ATCC number CCL-185™), human lung carcinoma, and Calu-1 (ECACC 93120818), human lung epidermoid cells, were chosen as model cancerous cell lines. BEAS-2B and A549 cell lines were purchased from American Type Culture Collection (ATTC) and Calu-1 cells were obtained from the European Collection of Authenticated Cell Cultures (ECACC).

A549 and BEAS-2B cells were cultured in (DMEM-F12) with 2 mM L-glutamine and 10% foetal bovine serum (FBS) at 37 °C in 5% CO_2. For Calu-1 cells, the growth conditions were the

 This journal is © The Royal Society of Chemistry 2017

Published on 08 August 2017. Downloaded by Dublin Institute of Technology on 04/09/2017 12:27:54.

same as for A549 and BEAS-2B, with the exception that the culture medium used was RPMI-1640, with 10% FBS and 2 mM L-glutamine supplement. A549 and Calu-1 cells were sub-cultured every 3 days, the BEAS-2B cell line every 4 days, until cells reached approximately 60–70% confluency.

AB (Alamar Blue) and MTT (3-(4,5-dimethylthiazol-2-yl)-2,5-diphenyltetrazolium bromide) assays and calculation of half-maximal effective concentration EC_{50} values

Both assays for the evaluation of cytotoxicity of the 100 nm PS-NH_2 to the chosen cell lines were conducted in the same plate. For cytotoxicity evaluation, each cell line was seeded onto 96-well plates at densities of 1×10^5, 5×10^4 and 3×10^4 cells per mL for 24, 48 and 72 hours, respectively. The cells were incubated at 37 °C in a 5% CO_2 humidified incubator for 24 h to achieve the initial attachment and desired confluency. For each cell line, six replicates of the positive (10% dimethyl sulfoxide (DMSO)) and negative (cell lines) control and particle exposures were used and 3 independent experiments were carried out from the same batch of the cells after different passages to evaluate toxicity.

PS-NH_2 solutions within the concentration range of 20 μM to 0.15 μM were freshly prepared in pre-heated cell medium with 10% FBS and 2 μM L-glutamine. For A549 and BEAS-2B cell lines, particles were prepared in DMEM-F12, whereas RPMI medium with 10% FBS and 2 μM L-glutamine was used for particle exposure to the Calu-1 cells.

Following 24 h initial attachment, the cells were rinsed with 100 μL per well of pre-warmed PBS and exposed to the test materials for 24, 48 and 72 h. After the desired exposure time, the cells were washed with PBS twice and exposed to the AB/MTT solution prepared in un-supplemented medium (A549 and BEAS-2B; DMEM-F12, Calu-1; RPMI) in the ratio of 5% [v/v] of AB and 10% [v/v] of MTT. Then the cells were incubated with the AB/MTT solution at 37 °C in 5% CO_2 for 3 h. A micro-plate reader (SpectraMax-M3, Molecular Devices, USA) was used to measure AB fluorescence emission at 595 nm. Following AB measurements, the AB/MTT solution was removed and the cells were washed with 100 μL per well of PBS twice. 100 μL per well of DMSO were added to 96-well plates and the plates were agitated at 200 rpm for 10 min. MTT absorbance was measured using the micro-plate reader at 570 nm. Data were transferred to SigmaPlot to fit the EC_{50} curve by using a four parameter sigmoidal fit.

Confocal laser scanning fluorescence microscopy

Confocal laser scanning microscopy (CLSM) was used to determine nanoparticle uptake and to observe cellular changes upon nanoparticle exposure as well as morphological changes in control cells over the exposure time. For each cell line, 1×10^5 cells per substrate were seeded onto glass bottom Petri dishes in the respective medium and incubated for 24 h at 37 °C in 5% CO_2. Following 24 h initial growth, cell medium was changed for the control cells and the test samples were exposed to 2.5, 1 and 0.6 μM of PS-NH_2 (calculated EC_{25} values) for A549, Calu-I and BEAS-2B, respectively and the cells were incubated for 24, 48 and 72 h. After the desired exposure time, the cells were rinsed with PBS three times and kept in PBS for confocal studies. CLSM images were taken by using a Zeiss Confocal Fluorescence Microscope (LSM 510 META, Carl Zeiss, Germany) with a ×63 oil immersion objective.

Raman microspectroscopy

In this study, Raman microspectroscopy is used to monitor cellular responses upon 100 nm PS-NH_2 exposure in cancerous (A549, Calu-1) and non-cancerous (BEAS-2B) cell lines to compare spectral fingerprints of molecular initiating events as well as cell death signatures. Cells were seeded onto CaF_2 discs at a density of approximately 16 000 cells per substrate and incubated for 24 h at 37 °C in 5% CO_2 in the respective medium for the cell line. Following initial attachment and growth, the cell medium was removed and the cells were rinsed with pre-warmed PBS. The cells were exposed to 2.5, 1 and 0.6 μM of 100 nm PS-NH_2 in cell medium supplemented with 10% FBS and 2 μM L-glutamine for A549, Calu-1 and BEAS-2B, respectively. The cells were incubated at 37 °C in 5% CO_2 for periods of 24, 48 and 72 h. For the control cells, the cell medium was replaced by fresh pre-warmed medium for a period equivalent to the PS-NH_2 exposure times. Following exposure, cell medium was removed and the cells were washed with 2 mL of PBS three times. 10% formalin was used as a fixative reagent and incubated with cells at room temperature for 10 min. After fixation, the cells were washed with PBS twice and kept in sterile dH_2O for Raman studies.

Throughout the study, a Horiba Jobin-Yvon LabRAM HR800 spectrometer, equipped with a 785 nm diode laser as a source, was used with a ×100 immersion objective (LUMPlanF1, Olympus, N.A. 1). The 520.7 cm^{-1} line of silicon was used to calibrate the spectrometer prior to spectral acquisition. A 300 lines per mm grating and a 100 μm confocal pinhole were chosen for all measurements and spectra were collected by using a 16 bit dynamic range Peltier cooled CCD detector. 20 point spectra from the cytoplasm of A549, Calu-1 and BEAS-2B cells and the corresponding controls for each exposure time were acquired for 2×30 seconds at each spot in the fingerprint region (from 400 cm^{-1} to 1800 cm^{-1}). Control cells incubated in the respective medium for up to 72 h were used to determine spectral changes as a result of particle exposure in PS-NH_2 exposed cells.

Data analysis

In order to observe the signatures of biochemical changes in cells upon PS-NH_2 exposure, the Raman data sets obtained from the exposed cells and their controls for different exposure times were transferred to Matlab (Mathworks, USA) for data analysis. All data sets were subjected to pre-processing prior to multivariate analysis. Briefly, a mild smoothing (Savitzky–Golay filter, 3rd order, 9 points) was applied and background was removed by using Classical Least Squares Analysis (CLSA) to remove contributions from the water in the immersion geometry.[24,35] Smoothed and background removed spectra were vector normalised prior to principal components analysis (PCA).

Published on 08 August 2017. Downloaded by Dublin Institute of Technology on 04/09/2017 12:27:54.

Intracellular reactive oxygen species (ROS) study

Generation of oxidative oxygen species in A549, Calu-1 and BEAS-2B cell lines for selected concentrations was evaluated by using the carboxy-H_2DCFDA dye. Cells were seeded onto 96-well plates at a density of 1×10^5 cells per well and incubated at 37 °C in 5% CO_2 for 24 h for initial attachment and growth. Following initial attachment, the cells were rinsed with 100 μL per well of PBS and 100 μL per well of carboxy-H_2DCFDA dye, prepared in PBS at a concentration of 10 μM, were added into the 96-well plates and the cells were incubated at 37 °C in 5% CO_2 for 30 min. After 30 min, the dye solution was removed from the plates and the cells were rinsed with 100 μL per well PBS twice. The cells were exposed to 0.6, 1 and 2.5 μM of PS-NH_2 prepared in pre-warmed cell medium with 10% FBS and 2 μM L-glutamine for BEAS-2B, Calu-1 and A549 cell lines, respectively. A 100 μM hydrogen peroxide (H_2O_2) solution was used as a positive control for all cell lines. The cells were incubated with test materials for 1, 2, 3, 4, 6 and 24 h. For positive and negative controls and PS-NH_2 exposure, 6 replicates are used in the same 96-well plate and 3 independent experiments were carried out from the same batch of the cells after different passages to evaluate the generation of reactive oxygen species (ROS). The plates were kept away from light throughout the experiment. The fluorescence emission of the oxidized DCFDA dye (excitation/emission: 485/535 nm) was measured at 535 nm by using a micro-plate reader (SpectraMax-M3, Molecular Devices, USA).

Lysosensor study

Lysosensor Green DND-189 was used to monitor lysosomal activity and aberrations in lysosomal activity for A549, Calu-1 and BEAS-2B upon exposure to 2.5, 1 and 0.6 μM concentrations of PS-NH_2. 10% DMSO was used as a positive control for all cell lines. Cells were seeded onto 96-well plates at a density of 1×10^5 cells per mL in pre-warmed medium supplemented with 10% FBS and 2 μM L-glutamine and incubated for 24 h at 37 °C in 5% CO_2. Following 24 h initial attachment, the cells are washed with PBS and exposed to test materials prepared in the respective medium for periods of 1, 2, 3, 4, 6 and 24 h. Lysosensor was prepared at a concentration of 2 μM in pre-warmed PBS. After the desired exposure time, the cells were washed twice with pre-warmed PBS and the cells were exposed to dye solutions for 30 min. After 30 min, plates were rinsed with PBS twice to remove unloaded dye and cells were kept in 100 μL per well PBS for the measurements. Lysosensor fluorescence emission was measured by using a micro-plate reader (SpectraMax-M3, Molecular Devices, USA) at 535 nm (Ex/Em: 488/535 nm).

Results and discussion

The cytotoxic effect of PS-NH_2 on cancerous and non-cancerous cell lines

The effect of 100 nm PS-NH_2 on cancerous (A549, Calu-1) and non-cancerous (BEAS-2B) cell lines was evaluated using commercially available and well-established cytotoxicity assays, AB and MTT.[36–38] Fig. 1 shows the dose dependent changes in cellular viability, at time points from 24 to 72 h, as determined by the AB (Fig. 1A, C and E) and MTT (Fig. 1B, D and F) assays. The cell viability assays are based on measurement of a fluorescent marker corresponding to a specific change in the whole cell population under investigation.[39] The AB assay provides information about the cell viability and proliferation while the MTT assay has been shown to have contribution from the mitochondrial activity of the cell.[36,40–43] Although MTT reduction can occur in different cellular regions, upon reduction of MTT dye to its fluorescent form by electron transfer after 25 min of incubation, around 25–45% of MTT reduction was shown to be associated with mitochondria by Bernas *et al.*[44] In the study of Maher *et al.*, MTT assay was found to be more sensitive than AB to the effect of exposure of cells to PAMAM dendrimers, which mainly localise in the mitochondria and cause changes in mitochondrial integrity.[45] Therefore, the MTT results can be interpreted in terms of functional changes of the mitochondria.

Even though the AB and MTT assays have different mechanisms for measuring toxic effects of the nanoparticles, in terms of applied dose, both assays provided comparable results for all cell lines and the toxicity progressively increased with increasing dose (from 0.15 to 20 μM) as seen in Fig. 1. When the AB response of A549, Calu-1 and BEAS-2B cells are compared, a general trend of increasing toxicity response in the order Calu-1 > BEAS-2B > A549 is observed (Fig. 1). For all three cell lines and exposure times, viability in the exposed cells is observed at around 100% for the lowest concentration of the PS-NH_2, while the percentage approaches zero for higher concentrations (Fig. 1A, C and D). The half-maximal concentrations for cellular viability (EC_{50}) were calculated by using a four parameter sigmoidal fit in SigmaPlot and the results are shown in Table 1. However, although the trend, Calu-1 > BEAS-2B > A549, remains the same for three cell lines, the AB assay does not show a significant difference in EC_{50} values between 48 and 72 h exposure for BEAS-2B cells (from 2.87 ± 0.41 to 3.20 ± 0.38 μM). When the confidence interval is calculated, EC_{50} is calculated to be in the range of 3.28–2.46 μM for 48 h and 3.58–2.82 μM for 72 h.

Notably, whereas the viability as measured by the AB assay for extended exposure times tends towards 10–0% for the cell lines, for the MTT assay, the increase in toxicity is observed to be less systematic for A549 and Calu-1 cells and the minimum viability, even at 72 h exposure, is observed around ~50–40% (Fig. 1B, D and F). This is indicative of sustained mitochondrial activity or increase in the number of mitochondria in cells upon exposure to PS-NH_2. In contrast, the viability of the BEAS-2B continues to reduce with increasing dose and extended exposure times, tending towards 10–0%, a similar profile to the AB response (Fig. 1A, C and E). From a pharmacological point of view, agonists can have partial or full efficacy on a receptor. While 'full agonism' can cause a reduction in viability to 0%, 'partial agonism' can cause the loss of viability to saturate at finite values, even at prolonged exposure times.[46] By analogy,

 This journal is © The Royal Society of Chemistry 2017

Published on 08 August 2017. Downloaded by Dublin Institute of Technology on 04/09/2017 12:27:54.

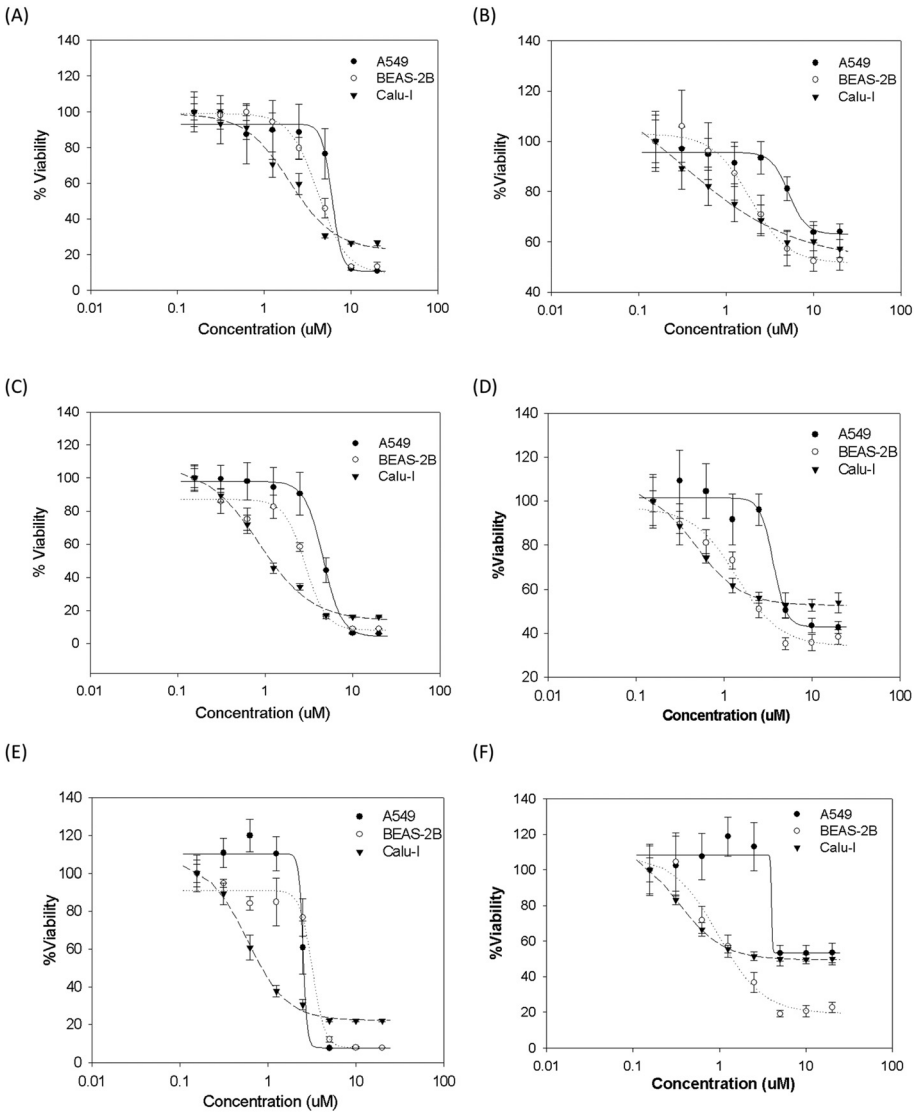

Fig. 1 Cytotoxicity of 100 nm amine-modified polystyrene nanoparticles (PS-NH_2) after 24 h (A and B), 48 h (C and D) and 72 h (E and F) exposures, as determined by the Alamar Blue (A, C and E) and MTT (B, D and F) assay, for A549, Calu-1 and BEAS-2B cell lines. The concentration range between 20 and 0.15 μM is used throughout the study. Data are expressed as % of control mean ± SD of three independent experiments.

Table 1 Calculated EC_{50} values with standard deviation for A549, Calu-1 and BEAS-2B cell lines from 24 to 72 h PS-NH_2 exposure

		EC_{50} values (μM)		
Cell lines	Viability assays	24 h	48 h	72 h
A549	AB	6.00 (±1.15)	4.62 (±0.13)	2.50 (±0.5)
	MTT	5.20 (±0.59)	3.63 (±0.55)	3.99 (±0.12)
Calu-1	AB	1.96 (±0.33)	0.85 (±0.11)	0.58 (±0.04)
	MTT	0.30 (±0.42)	0.47 (±0.03)	0.33 (±0.01)
BEAS-2B	AB	4.17 (±0.24)	2.87 (±0.41)	3.20 (±0.38)
	MTT	2.00 (±0.06)	1.39 (±0.27)	0.97 (±0.18)

the MTT response in A549 and Calu-1 can be described as "partial agonism" as the viability only goes to about 50%, whereas in BEAS-2Bs, there is almost a full loss of viability.

In recent years, the mechanisms underlying the toxicity of nanoparticles have been widely studied and various contributions have been identified, such as induction of oxidative stress upon nanoparticle uptake, cascades of inflammatory responses, counteracted by natural cell defense mechanisms (*e.g.* antioxidants).[15,21,22,31,32,34,47,48] In the case of the PS-NH_2, partial agonism determined by the MTT assay shows evidence of more than one mechanism governing the toxic response. The partial agonistic MTT response for A549 and Calu-1 cells can also be attributed to more effective defense mechanisms, such as more effective antioxidant quenching of ROS in cancer cell lines compared to non-cancerous cell lines.[49] Conversely, for the BEAS-2B cells, the similar response and systematic changes ('full agonistic response' for all exposure times) determined by both assays can be related to the prevalence of one toxic pathway leading to cell death.

Published on 08 August 2017. Downloaded by Dublin Institute of Technology on 04/09/2017 12:27:54.

Morphological changes in cancerous and non-cancerous cells upon PS-NH_2 exposure

Morphological changes also provide valuable information about the cell viability and overall cell health. In the case of cellular stress and activation of cell death pathways leading to apoptosis and necrosis, significant changes occur in the overall cell structure such as cell shrinkage or swallow, alterations and aberrations in the cell membrane, cell blebbing or budding and formation of stress related granular structures.[50–52] In order to observe morphological effects of the systematic changes on BEAS-2B cells upon PS-NH_2 exposure, CLSM was employed to visualise exposed cells compared to their corresponding controls from 24 to 72 h (Fig. 2). Extending exposure times from 24 to 72 h, control cells are observed to be affected by nutrient consumption[53] and several morphological changes are observed in the cell membrane and cytoplasm. Cellular stress related lipid granules were observed after 48 h (indicated by an arrow in Fig. 2) and the change in the cellular morphology is observed significantly after 72 h. For PS-NH_2 exposed cells, 0.6 μM concentrations of PS-NH_2 were chosen as a sub-lethal dose (~EC_{25} values at 24 h exposure determined by MTT) for the CLSM study. After 24 h particle exposure, PS-NH_2 are observed to be mainly localised in the perinuclear region. After 72 h, excessive amounts of PS-NH_2 are observed in the cytoplasmic area and morphological changes become highly visible. For all exposure times, the formation of stress related lipid granules was observed to be increased upon particle exposure. Compared to their controls for each exposure time, significantly higher distortion in the cell structure is observed.

Consistent with the known trafficking of PS nanoparticles, after 24 h exposure, the particles are observed to be in the perinuclear region which shows the localisation of the nanoparticles in the endoplasmic reticulum. With the extending exposure times, although uptake and trafficking of the PS-NH_2 continue and the amount of the particles increase inside the cell, no localisation of the particles are observed in the nuclear region.[22]

Raman microspectroscopic evolution of the spectral markers of toxicity in cancerous and non-cancerous cell lines

In order to investigate in more detail the systematic changes within PS-NH_2 exposed BEAS-2B cells determined by the MTT assay and CLSM, Raman spectra were acquired from 20 points within the cytoplasm of the exposed cells and their corresponding controls. For the Raman study, the ~EC_{25} at 24 h exposure determined by the MTT assay (0.6 μM concentration of PS-NH_2) was chosen as a sublethal dose at which the time dependent changes in the cell line were observed.

The spectral changes in BEAS-2B, the non-cancerous cell line, upon PS-NH_2 exposure from 24 to 72 h were evaluated by using PCA. The scatter plots of PCA obtained from comparison of the cytoplasm of the exposed and unexposed BEAS-2B cells after 24, 48 and 72 h particle exposure are provided in ESI Fig. S1.† For all exposure times, exposed cells clearly separated from their controls according to PC1, with increasing explained variance with increasing exposure times. In all cases, control cells are observed to form more compact clusters, which indicate higher variance in particle exposed cells, as might be expected. The explained variances are calculated to be 62, 84 and 89% for 24, 48 and 72 h, respectively, which indicates the significant changes in cell composition upon PS-NH_2 exposure. The loadings of PC1 for control *versus* PS-NH_2 exposed BEAS-2B cells, from 24 to 72 h, are provided in Fig. 3. In each loading, negative features (PC < 0) represent

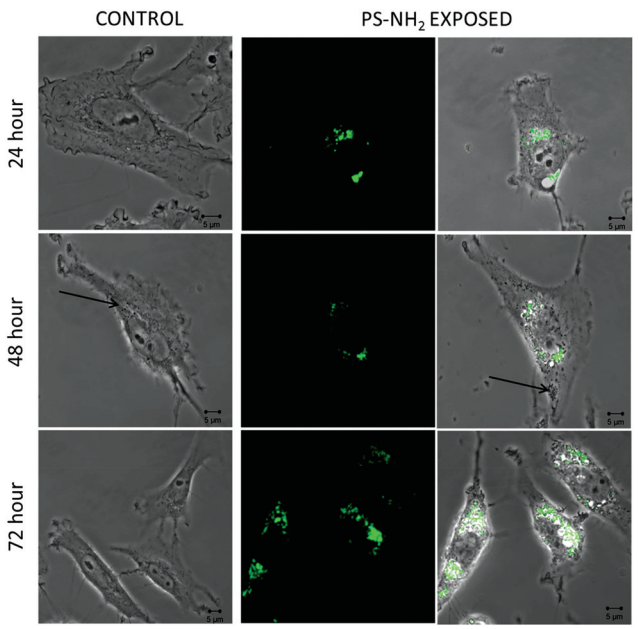

Fig. 2 CLSM images of BEAS-2B cells and BEAS-2B cells exposed to 100 nm aminated polystyrene nanoparticles (indicated by green fluorescent) from 24 to 72 hours. ×60 magnification.

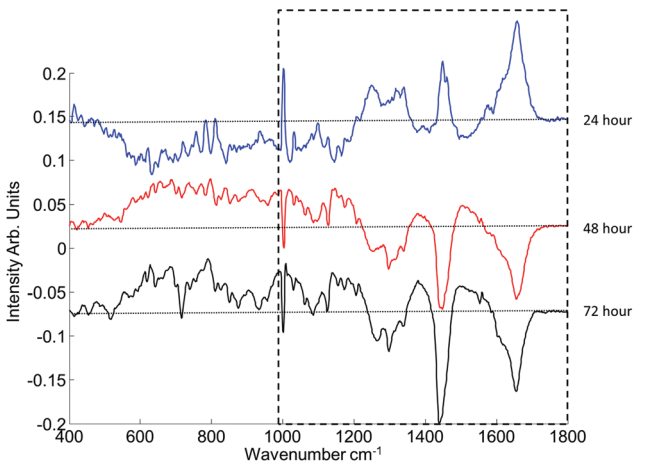

Fig. 3 Loadings of the first component of PCA (PC1), each exposure time is indicated by a colour from 24 h to 72 h as following: blue, red and black. The positive side of the loadings represents the spectral features of the particle exposed cells (0.6 μM of PS-NH_2), while the negative side represents the control cells for each loading. Loadings are offset for clarity and the dotted line represents the zero '0' point for each loading. The changing features with extended particle exposure times are indicated by a black dashed area.

This journal is © The Royal Society of Chemistry 2017

Published on 08 August 2017. Downloaded by Dublin Institute of Technology on 04/09/2017 12:27:54.

the dominant features of the cytoplasm of control cells and positive features (PC > 0) represent the features of PS-NH_2 exposed cells. The most significant changes in the loadings are observed in the range between 1000 and 1800 cm^{-1} and are indicated by black dashes (band assignments are provided in Table S1†). When the loadings of PC1 for different exposure times are compared, significant differences are observed between 24 and 48 h particle exposure, including inversion of bands between control and exposed cells (Fig. 3). After 24 h exposure, protein (1003 cm^{-1}, phenylalanine (Phe); 1033 cm^{-1}, Phe; 1248 cm^{-1}, amide III of proteins, also attributed to nucleic acids, guanine (G) or cytosine (NH_2); 1339 cm^{-1}, Phe, tyrosine (Tyr); 1658 cm^{-1} amide I (α-helix)[54] band of proteins) and lipid bands (1440 cm^{-1}, lipids)[54–56] are observed in the positive features of the PC1, which indicates an increased amount of protein and lipids in PS-NH_2 exposed compared to control cells. Although the highest peak observed in the range of 1600 to 1700 cm^{-1} is identified at 1658 cm^{-1}, the region can have many contributions in this region from lipids (C═O and/or C═C band) and also some residual water (bound of semi-bound –OH).[57,58] The possible contributions in the range and their assignments are provided in Table S1.† The increased signatures of proteins in particle exposed cells compared to their corresponding controls can be attributed to the changes in the protein template and formation of altered protein structures and also changes in post-translational modifications of the proteins and problems in protein degradation mechanisms due to the changes in cell signalling upon nanoparticle uptake.[59–61] Also, it can be attributed to formation of more Raman active proteins or conformational changes.[62] Uptake and removal mechanism of the nanoparticles also leads to the formation of lipid based structures such as lysosomes to facilitate cellular trafficking of the nanoparticles, which results in an increase in lipid bands. Moreover, formation of stress related lipid granules in the cytoplasm observed with CLSM can contribute to the increase in the lipid band at 1440 cm^{-1}.

After 48 and 72 h exposure, the most prominent bands are observed in the negative features of loading 1, which represents a higher amount of the corresponding cellular constituents in control cells compared to PS-NH_2 exposed cells. The lipid and protein bands are inverted to negative features of the loading 1 which indicates damage and loss of the protein and lipids in particle exposed cells. The increase of the features in the loading from 48 to 72 h indicates the progress of the cascade of events in the cell, resulting in further degradation in protein and lipid structures due to the toxicity of the particles.

The decrease in lipid composition of the cells after 48 and 72 h exposure can be attributed to the lysosomal aberrations due to long exposure times. The uptake mechanism of the PS-NH_2 nanoparticles is known to be endocytosis. Briefly, particles are taken up by endosomes in the first 4 h and carried to lysosomes within 12 h, which are engulfed by Golgi apparatus or endoplasmic reticulum after 24 h.[22] However, amine groups located on the surface provide a cationic surface charge to PS-NH_2. Therefore, particles create a proton-sponge effect in the early endosomes and lysosomes which cause protonation in lysosomes.[15,63–67] Reduction in protein content for these exposure times can be an indicator of follow up damage in the exposed cells due to oxidative stress. After 72 h exposure, the band at 719 cm^{-1} (membrane phospholipid head, phosphatidylcholine)[54–56] can be used to track damage to membrane integrity and cellular death phase.

A doublet of peaks at around 785 cm^{-1} (nucleic acids) and 810 cm^{-1} (RNA), associated with the changes in the nucleic acid content in the cytoplasm, has previously been identified as a potential marker for oxidative stress in the Raman signatures of nanoparticle exposed cells.[21] The increasing amount of the nucleic acid bands in the cytoplasm of the particle exposed cells compared to control cells can be attributed to the changes in cytoplasmic RNA and accumulation of non-coding RNAs in the cytoplasm due to oxidative stress. However, they are only weakly observed as positive features of the loading after 24 h particle exposure are not evident at all at the prolonged exposure times, which shows a lack of RNA accumulation in the cytoplasm of the exposed BEAS-2B cells for longer time points.

As seen in Fig. 3, the spectral changes in BEAS-2B cells are found to be systematic after 24 h particle exposure, which correlates with the full agonistic response determined by AB and MTT assays and evolving changes in CLSM. Therefore, the significant changes in the spectroscopic signatures between 24 and 48 h particle exposure (with an increase in explained variance from 62 to 84%) can be related to initiation of toxic events (molecular initiation event (MIE)) and the lower increase in the explained variance (from 84 to 89%) from 48 to 72 h can be attributed to the cascade of following toxic responses in the cell.

The differences encountered in AB and MTT assays between BEAS-2B, non-cancerous, and A549 and Calu-1, cancerous, cell lines were also investigated using Raman microspectroscopy. The partial agonistic response obtained by the MTT assay for A549 and Calu-1 cells can be attributed to the differences in mitochondrial functionality following the nanoparticle uptake. In order to observe the differences between cell lines in terms of spectroscopy, 20 point spectra from the cytoplasm of different individual cells were acquired for each exposed cell line and their corresponding controls. For the Raman study, concentrations of 2.5, 1 and 0.6 μM PS-NH_2 were chosen as sub-lethal doses (~EC_{25} values at 24 h exposure) to observe time dependent changes in the cell lines.

The 72 h exposure time was chosen to compare cellular responses as more obvious changes ('full agonistic response' for BEAS-2B, 'partial agonistic response' for A549 and Calu-1) are observed for the MTT assay results at this time point (Fig. 1). PCA was applied pairwise between controls and particle exposed cells after 72 h exposure. The scatter plots of the PCA of the cytoplasm of exposed and control cells for A549 and Calu-1 cells after 72 h are shown in ESI Fig. S2.† The exposed cells differentiate according to PC1 from their controls 43% and 46% for A549 and Calu-1 cells, respectively. For BEAS-2Bs, exposed cells largely differentiate from controls (explained variance 89%, Fig. S1†). Fig. 4 shows the first load-

Published on 08 August 2017. Downloaded by Dublin Institute of Technology on 04/09/2017 12:27:54.

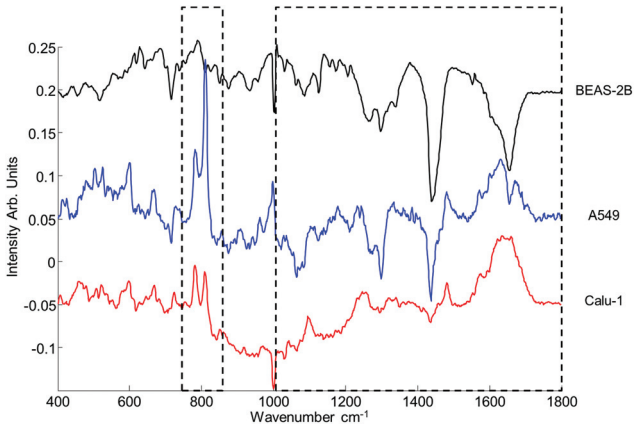

Fig. 4 First loadings of PCA of cytoplasm of control and 72 hour particle exposed cells for BEAS-2B, A549 and Calu-1 cell lines, respectively; loadings are offset for clarity and the dotted line represents the zero '0' point for each loading. The positive side of the loadings (PC > 0) represents the spectral features of the particle exposed cells, while the negative side (PC < 0) represents the control cells for each loading. The areas with changing features between cell lines are indicated by dashed lines.

ings of PCA for BEAS-2B, A549 and Calu-1 cells, corresponding to the cytoplasm. When the first loadings are compared, similar trends in the spectral range from 1000 to 1800 cm^{-1} for A549 and BEAS-2B cells are observed, which can be attributed to similarities in the cascade of events for one type of toxic pathway which can also be attributed to the similarities in the full agonistic cellular response determined by the AB assay. The spectral range from 1000 to 1800 cm^{-1} of the so-called fingerprint region includes many characteristic bands related to protein and lipid content of the cells. When the chosen range is considered, for all cell lines, loadings are dominated by negative features. The bands at 1266 cm^{-1} (amide III-α helix), 1298 cm^{-1} (lipids) and 1438 cm^{-1} (lipids and proteins) are observed as positive features of the loading for the Calu-1 cells. The band at 1658 cm^{-1}, which can specifically be attributed to the amide I (α-helix) of proteins,[54] is observed as negative features of the loadings for BEAS-2B and A549 cells, whereas the peak manifests as a positive feature for the Calu-1 cells, indicating a lower amount of damage in amide I band of the proteins in the Calu-1 cells compared to the other cell lines. For A549 cells, the positive features in the range from 1600 to 1700 cm^{-1} can be attributed to partial aberrations in protein and lipid band (C═C and/or C═O) characteristics of this region. The inverted structure of these bands can be attributed to damage of protein and lipid structures in particle exposed cells after 72 h. Although the cell lines are different from each other, the spectral signatures of cell damage leading to cell death in later stages are found to be similar and cell damage upon toxicity can be determined using Raman microspectroscopy which can be used to utilize a single step analysis of cell–nanoparticle interaction for different cell lines.

Although a general trend is observed in the AB responses and spectral signatures of cell damage for all three cell lines in the higher wavenumber region of the fingerprint, a significantly different trend is observed for the lower wavenumber region, 785–810 cm^{-1}, which indicates the presence of different molecular initiating events, as well as the presence of a secondary toxic pathway leading to cell death upon toxic nanoparticle exposure.

The prominent peaks at 785 cm^{-1} (nucleic acid) and 810 cm^{-1} (RNA), in the loadings corresponding to the cytoplasm of A549 and Calu-1 cells are indicative of nucleic acid alterations in the cytoplasm due to oxidative stress, as previously discussed for A549 cells.[21] However, the peaks are absent in the loading of BEAS-2B cells after 72 h exposure. Although ROS such as hydrogen peroxide (H_2O_2), superoxide anion ($O^{2\bullet-}$) and hydroxyl radicals ($HO^{\bullet}$) are known to be Raman inactive and are consumed in cells quickly after they are produced,[68,69] the 785 and 810 cm^{-1} bands can be used to track oxidative stress inside the cells in a completely label free manner.[21]

The nucleic acid bands in the cytoplasm have been identified as a signature of formation and accumulation of noncoding RNAs due to oxidative stress upon particle exposure.[21] In order to further explore this process in the cytoplasm of the different cell lines, the ROS levels of A549, Calu-1 and BEAS-2B cells were measured by using the carboxy-H_2DCFDA dye (Fig. 5). The concentrations for ROS measurements were kept the same as the concentrations used for the Raman study for each line (0.6, 1 and 2.5 μM for BEAS-2B, Calu-1 and A549, respectively) in order to observe the ROS levels corresponding to the doublet of peaks. The results show significantly lower ROS formation in the BEAS-2B cells, which is consistent with the absence of the double peak in the lower wavenumber region. For this reason, the formation of ROS can be identified as a molecular initiating event for the A549 and Calu-1 cell lines, which leads to cell damage and ultimately cell death.

In order to see earlier effects of the molecular initiating event for the different cell lines, spectral changes were also

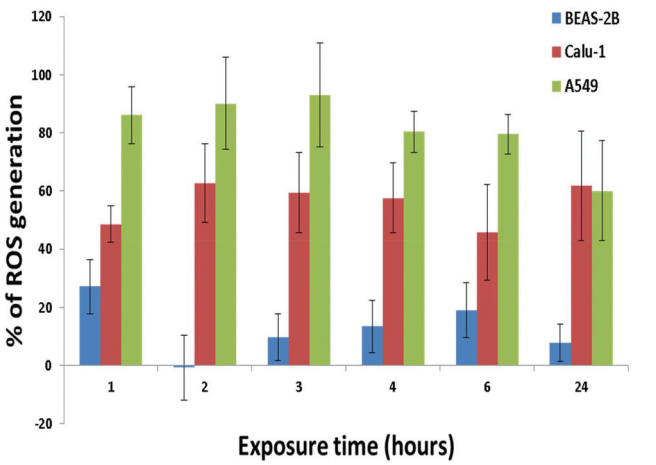

Fig. 5 % of reactive oxygen species (ROS) generation compared to controls for A549, Calu-1 and BEAS-2B cell lines after 1, 2, 3, 4, 6 and 24 h PS-NH_2 exposure. The concentrations used for BEAS-2B, Calu-1 and A549 are 0.6, 1 and 2.5 μM, respectively.

This journal is © The Royal Society of Chemistry 2017

Published on 08 August 2017. Downloaded by Dublin Institute of Technology on 04/09/2017 12:27:54.

investigated at shorter exposure times (24 and 48 h) and pairwise PCA of cytoplasm corresponding to the exposed cells and their controls was carried out. The scatter plots of PCA of cytoplasm of exposed and control cells are provided in ESI Fig. S1 (A and B†) for BEAS-2B and Fig. S3† for A549 and Calu-1 cells after 24 and 48 h. The explained variance between control and exposed cells according to PC1 increases to 64 and 59% for A549 and Calu-1 cells and PS-NH_2 exposed BEAS-2Bs differentiate from their controls 84% after 48 h exposure. The increase in explained variance after 48 h exposure compared to 72 h for A549 and Calu-1 cells can be attributed to higher stress in the control cells due to rapid consumption of medium by metabolically active cancer cell lines.[70] A representative example of the morphological changes in control cells after 48 and 72 h exposure, as seen by white light microscopy, is shown for A549 cells in ESI Fig. S4.† Changes in cell shape, membrane integrity and formation of lipid vesicles, relating to the oxidative stress, are observed with increasing exposure time. When the exposure time is reduced to 24 h, A549, Calu-1 and BEAS-2B cells differentiate from the corresponding controls according to PC1, explaining ~50–60% for all cell lines. Fig. 6 shows the loadings of PC1 corresponding to the cytoplasm of exposed and control cells after 24, 48 and 72 h for A549 (A) and Calu-1 (B) cells. A549 and Calu-1 cell lines show similar responses in the lower wavenumber region and the double peak at 785 and 810 cm^{-1} is prominently observed for all exposure times (Fig. 6 (A and B)). The change in the bands at 785 and 810 cm^{-1} also shows similarity in terms of the intensity ratio of the 785/810 cm^{-1} bands, which indicates comparable changes in RNA accumulation for both cell lines (Fig. 6). Conversely, the double peak, 785 and 810 cm^{-1}, is absent in the loading of PC1 of the BEAS-2B cell line after 48 h exposure (Fig. 3). When the exposure time is reduced to 24 h, the double peak has low intensity, which indicates the production of ROS in low levels and rapid consumption for the BEAS-2B cell line. The significantly higher intensity of 785 and 810 cm^{-1} bands can be attributed to higher amounts of accumulated nucleic acids in the cytoplasm of A549 and Calu-1 cells compared to BEAS-2B cells, consistent with the higher levels of ROS observed (Fig. 5).

When different cell lines are compared in the higher wavenumber region of the fingerprint, above 1000 cm^{-1}, after 24 and 48 h exposure, similar trends are observed in A549 and Calu-1 cells, which are mainly an increase or a decrease in protein and lipid related bands in particle exposed cells compared to their corresponding controls (Fig. 6(A) and (B)). However, BEAS-2B cells show a significant change between 24 and 48 h (Fig. 3), which can be attributed to a more rapid and single step mechanism in the cytotoxic response rather than multiple mechanisms. The rapid toxic response can be related to the full agonistic mechanism of the BEAS-2B cells (Fig. 1) determined by the AB and MTT assays, which is also consistent with the less effective defence mechanisms of non-cancerous cell lines.[71]

As seen in Fig. 6(A) for A549 cells, after 48 h exposure, the loading of PC1 is dominated by negative features above 1000 cm^{-1}. The bands at 1266 cm^{-1} (amide III/α-helix), 1298 cm^{-1} (lipids), 1438 cm^{-1} (lipids, proteins) and 1658 cm^{-1} (amide I (α-helix)) are observed in the negative features of the loadings, which is consistent with damage to protein and lipid content of the exposed cells. The damage and loss in lipid composition of the cell can be attributed to protonation in lysosomes, lipidosis and ultimately lysosomal rupture as well as higher ROS levels in the cell upon PS-NH_2 exposure. The oxidative stress also causes alterations and damage to proteins in the cytosolic region of the exposed cells. When the exposure time is reduced to 24 h, A549 cells show changes in the same features as the loadings of 48 h, with less damage to protein and lipid structures. For the Calu-1 cell line, similar to the A549 cells, the loading of PC1 is dominated by negative features above 1000 cm^{-1} (Fig. 6(B)). The bands at 1266 cm^{-1} (amide III/α-helix), 1298 cm^{-1} (lipids) and 1438 cm^{-1} (lipids, proteins) are observed in the negative features of the loading. However, the range from 1600 to 1700 cm^{-1} of the Calu-1 cells shows significant differences compared to that of A549 cells. This region, as a broad band formed by multiple sub-bands, can be related to different molecular vibrations such as C–C, C═O[54] and indicates the presence of lipid and proteins (Table S1†). Although the band at 1658 cm^{-1} (amide I (α-helix))

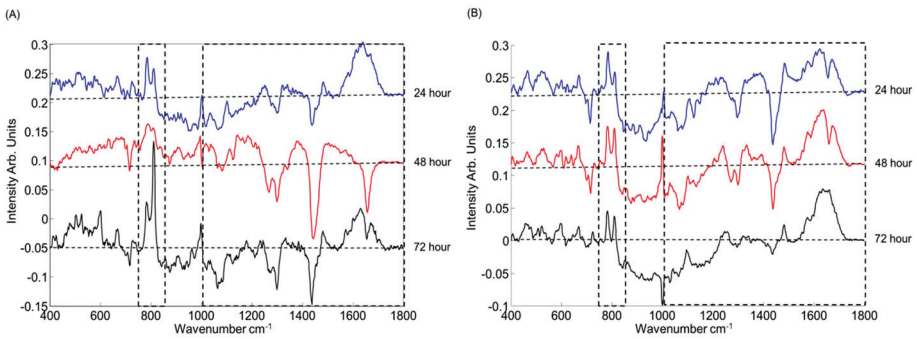

Fig. 6 Comparison of the first loadings of PCA of cytoplasm of control and particle exposed A549 (A) and Calu-1 (B) cell lines after 24, 48 and 72 hour particle exposure; loadings are offset for clarity and the dotted line represents the zero '0' point for each loading. The positive side of the loadings represents the spectral features of the particle exposed cells, while the negative side represents the control cells for each loading. The changing features between cell lines are indicated with dashed lines.

Published on 08 August 2017. Downloaded by Dublin Institute of Technology on 04/09/2017 12:27:54.

can be identified as a negative feature in the loading, the general changes in the protein content of exposed cells are observed as positive features after 24 and 48 h exposure, which indicates a higher amount of proteins as well as more Raman active proteins in the PS-NH_2 exposed cells compared to the corresponding controls. The later effect on protein structures compared to lipid content can be explained by a cascade of events in the cell upon toxic particle exposure. The onset of lipidosis, change in pH gradient and ROS formation can impact on proteins at later stages, compared to the lipid based changes in the earlier stages. Moreover, the change in the spectral markers of proteins and lipids in Calu-1 cells with increasing exposure time is not observed to be as significant as A549 cells which can be attributed to a slower cytotoxic response.

Conversely, for the BEAS-2B cells, the formation of the cellular damage cannot be attributed to ROS due to low levels of measured ROS and the absence of the double peak at 785 and 810 cm^{-1}, even though similar signatures of cell damage response are observed in the range above 1000 cm^{-1} with A549 and Calu-1 cells. Although ROS is one of the mechanisms for cellular damage, other toxic pathways can be identified for cell death. pH gradient of the cells can have a significant contribution to damage in biochemical composition of the cells as well as effecting the working mechanism of the cellular compartments.[72] The levels of the protonation in acidic organelles such as endosomes and lysosomes were measured using the Lysosensor dye. Lysosensor is known to be a pH dependent dye which quantifies the lysosomal content. As seen in Fig. 7, BEAS-2B cells show a continuous protonation in lysosomes over a 24 h period. In contrast, A549 and Calu-1 cells show fluctuations in protonation. Changes and fluctuations in the amount of protonated lysosomes can be explained by three different events occurring in the cell upon PS-NH_2 exposure. First, the proton pump effect can be initiated by PS-NH_2 uptake into cells and formation of endosomes. After 3 to 4 h exposure, fusion of endosomes in lysosomes occurs and lysosomal protonation can initiate the second source of protonation, while the third can be related to lysosomal rupture. The fluctuations in protonation also show these additional protonation stages such as lysosomal rupture in A549 and Calu-1 cells compared to BEAS-2B cells. The lysosomal rupture has a significant effect on ROS formation, which ultimately affects the RNA in the cytoplasm and results in accumulation of the noncoding RNAs. Although there are fluctuations in the levels for A549 (A) and Calu-1 (B) cells, the lysosomal protonation can contribute to cellular toxicity, in concert with ROS formation. On the other hand, the main reason for PS-NH_2 toxicity to BEAS-2B cells can be a continuous proton pump effect which affects the internal pH and ultimately pH gradient in the cytosolic region. Continuous changes in the internal pH can show a significant effect on the working mechanism of the mitochondria which needs a proton gradient for energy production and full functionality.[73] The effect of PS-NH_2 on the mitochondria of BEAS-2B cells can also be seen from the MTT response and full agonistic feature of PS-NH_2 for the BEAS-2B cell line.

Overall, the cellular toxicity of PS-NH_2 for A549 and Calu-1 cells can be associated with two mechanisms, whereas BEAS-2B shows only one main mechanism. Briefly, after PS-NH_2 are taken up by A549 and Calu-1 cells, they give rise to the proton pump effect in lysosomes, which elicits a partial MTT response and changes mitochondrial activity as one mechanism. The ROS formation due to subsequent lysosomal rupture can be identified as the main mechanism which leads to cell damage and death, resulting in the full agonistic AB response. Conversely, BEAS-2B cells retain the lysosomal integ-

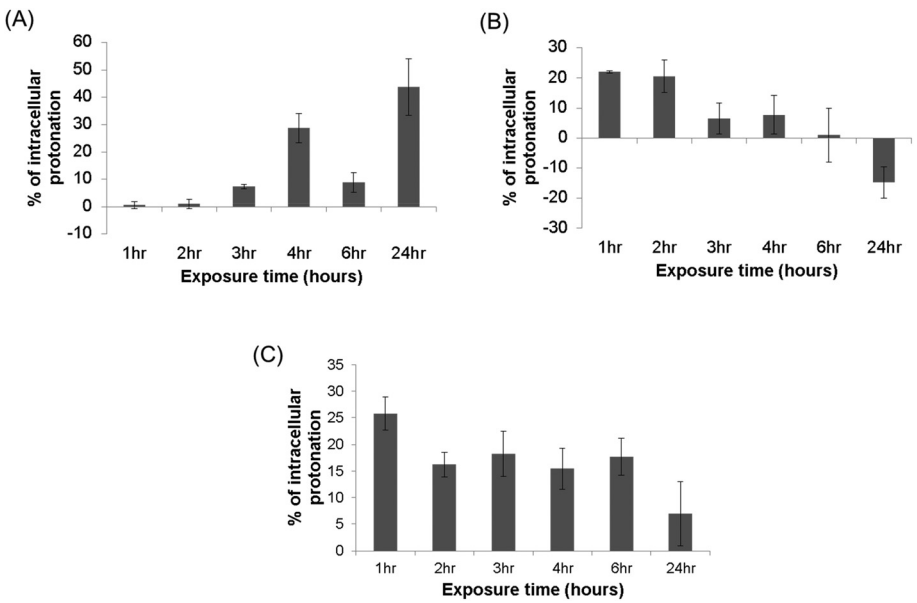

Fig. 7 Changes in lysosomal protonation measured by Lysosensor activity in A549 (A), Calu-1 (B) and BEAS-2B (C) cell lines.

 This journal is © The Royal Society of Chemistry 2017

Published on 08 August 2017. Downloaded by Dublin Institute of Technology on 04/09/2017 12:27:54.

rity and elicit a full agonistic response in MTT. The proton pump effect and the changes in mitochondrial function leads to cell death. A schematic representation of the different pathways for different cell lines can be seen in Fig. 8.

Previous studies have shown the higher susceptibility of the lysosomal-mediated cell death in cancer cell lines compared to the normal cells.[74] The relatively larger size of the lysosomes in the cancer cells are shown to make the lysosomal structure more fragile which makes the lysosomal alterations more common in cancerous cells.[75] In the study by LeGendre *et al.*, anticancer effects of the (−)-oleocanthal, a phenolic compound in olive oil, has been demonstrated on the cancerous and non-cancerous cell lines and it has been found to selectively induce cell death in cancer cell lines due to fragility of the lysosomes and changes in lysosomal membrane permeabilization.[75] Therefore, the differences between cancer and non-cancerous cell lines observed by Raman microspectroscopy which can be attributed to lysosomal rupture resulting in cell death as a second mechanism for cancerous cell lines, A549 and Calu-1, can also be attributed to lysosomal alterations due to larger size and fragility of the lysosomes. The CLSM images of the PS-NH_2 exposed cells also show a different distribution of the nanoparticles inside the cytoplasmic area after 24 h for A549 and Calu-1 cells compared to BEAS-2B cells (ESI Fig. S5†). For the A549 (A) and Calu-1 (B), PS-NH_2 are observed to be more spread in the cytoplasm, whereas the particles are observed to localise in the perinuclear region for BEAS-2B (C) cells which indicates evidence of common lysosomal rupture in the cancerous cell lines.

In this study, Raman microspectroscopy is shown to provide information in a rapid way with high sensitivity regarding overall cellular health, lysosomal and mitochondrial changes, changes in the biochemical composition of the cell, oxidative stress, from early stage particle exposure to cell death, as a function of time, in a range of cell lines. Raman microspectroscopy can be applied to different areas, from *in vitro* toxicology to medicinal chemistry,[21,76–80] as a high content screening technique, due to the multifaceted information contained in the fingerprint region and the technique can potentially replace the cellular and biochemical assays which require the use of multiple assays with multiple labels. The use of labels for the evaluation of cellular processes as well as localisation studies has been widely studied in different areas.[15,81,82] However, the labels are known to be specific to one cellular event, whereas a complex series of events can take place inside the cell as a response to a single stimulus. The specificity of the labels brings the requirement of the use of multiple assays which is inefficient in terms of cost and time. Notably, when the complexity of cells, tissues and higher animal models are considered, the amount of assays and analysis required to complete the picture of interaction mechanisms and efficacies and responses significantly retards the whole process for pharmaceutical and medical applications. As it is label free, Raman microspectroscopy uses the intrinsic properties of the biochemical constituents of the cells and spectral markers of subcellular events occurring inside the cell and allows the detection of the changes without targeting a specific molecule or event. For example, the cytotoxicity assays used in this study are based on measurement of the resorufin (pink and highly fluorescent) and formazan (purple) products inside the cell which are produced as a result of resazurin and MTT reduction by AB and MTT assays, respectively.[40,41] Therefore, although conventional cytotoxicity assays such as AB and MTT provide valuable indications of the response of a cell population, they are based on the measurement of a specific marker and do not provide any information on the mechanism of action or response pathways. Differing responses are commonly obtained from different assays, and the collective responses of multiple assays are not readily interpretable. As a high content screening technique, Raman microspectroscopy, can elucidate the mechanism of action and different pathways leading to toxicity. The particle dependent (ROS) and cellular dependent (damage in protein and lipid structures, which gives information about cellular viability) spectral markers can be applied to predict nanoparticle toxicity. The consistencies in the spectral markers of the particle and cellular dependent events can be converted into more quantitative measurements with the analysis of spectral marker intensities *versus* dose and time. Moreover, further refinements of the data analysis and quantification protocols can be achieved by using more sophisticated data mining methods such as PC-LDA (Principal Component-Linear Discriminant Analysis) and Partial Least Squares Regression analysis (PLSR) to achieve improved differentiation and quantification.

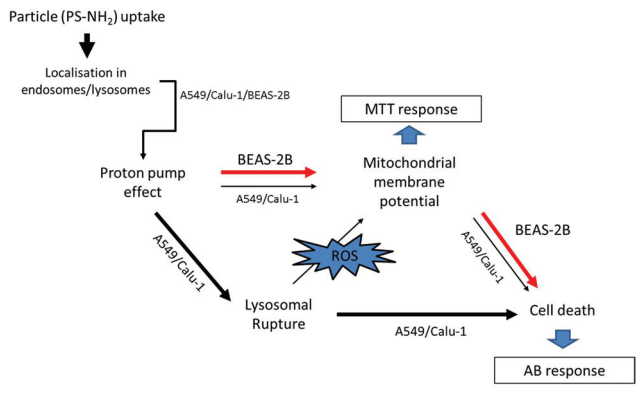

Fig. 8 Schematic representation of different cell death pathways for A549, Calu-1 and BEAS-2B cell lines. The pathway for the BEAS-2B cell line is indicated by red arrows, while that for A549 and Calu-1 is represented by black arrows.

Conclusion

Although conventional cytotoxicity assays, AB and MTT, provide valuable information about the toxicity of PS-NH_2, the techniques have been shown to be limited by the nature of the measurement methodology. The individual technique relies

Published on 08 August 2017. Downloaded by Dublin Institute of Technology on 04/09/2017 12:27:54.

on the colorimetric changes on a specific marker. The varying results obtained from different assessments, which reflects the measurement of a different specific marker, can show a high impact on the evaluation of the nanoparticle toxicity and the reliability of the results. However, Raman microspectroscopy can provide deeper insights into toxic pathways by using intrinsic properties of biological molecules which are produced and consumed during cellular events. Upon exposure to a toxicant, spectral markers of the molecular initiating events and the subsequent cascade of events can be determined using Raman microspectroscopy. The spectral markers of toxicity obtained by Raman microspectroscopy can be observed in multiple cell lines and allow the prediction of the mechanism of action of the nanomaterial.

This study has further demonstrated the different cellular responses and mechanisms leading to cell death between cancerous and non-cancerous cell lines can be differentiated by using the spectral markers of the cellular toxic events. The doublet peak, 785–810 cm^{-1}, is identified as a signature of ROS related changes in the biochemical composition of the cell upon a toxicant exposure and the changes upon activation of the cell death mechanism has been identified with the region over 1000 cm^{-1} with the changes in protein and lipid structures.

The proof of concept study has demonstrated the consistency of the Raman spectroscopic signatures at a subcellular level, as a result of cell exposure to nanoscale toxicants, for the example of the commercially available PS-NH_2. It demonstrates that the signatures of the initial responses to oxidative stress are consistent in different cell lines, and furthermore that the subsequent cellular responses can be interpreted in terms of characteristic signatures, including those of the cellular defence mechanisms, which are potentially quantifiable as a function of dose and/or exposure time. The confocal spectroscopic technique therefore provides a holistic view of the initiation stage of the toxicity as well as the cellular response in a high content, label free readout.

Conflicts of interest

The authors declare that there are no conflicts of interest.

Acknowledgements

This work was supported by Science Foundation Ireland Principle Investigator Award 11/PI/1108.

References

1 W. T. Godbey, K. K. Wu and A. G. Mikos, *Proc. Natl. Acad. Sci. U. S. A.*, 1999, **96**, 5177–5181.
2 G. Tosi, B. Bortot, B. Ruozi, D. Dolcetta, M. A. Vandelli, F. Forni and G. M. Severini, *Curr. Med. Chem.*, 2013, **20**, 2212–2225.
3 S. K. Nune, P. Gunda, P. K. Thallapally, Y.-Y. Lin, M. L. Forrest and C. J. Berkland, *Expert Opin. Drug Delivery*, 2009, **6**, 1175–1194.
4 I. Brigger, C. Dubernet and P. Couvreur, *Adv. Drug Delivery Rev.*, 2012, **64**(Supplement), 24–36.
5 G. Oberdörster, A. Maynard, K. Donaldson, V. Castranova, J. Fitzpatrick, K. Ausman, J. Carter, B. Karn, W. Kreyling, D. Lai, S. Olin, N. Monteiro-Riviere, D. Warheit and H. Yang, *Part. Fibre Toxicol.*, 2005, **2**, 8.
6 A. E. Nel, L. Madler, D. Velegol, T. Xia, E. M. V. Hoek, P. Somasundaran, F. Klaessig, V. Castranova and M. Thompson, *Nat. Mater.*, 2009, **8**, 543–557.
7 OECD, OECD Guidelines for the Testing of Chemicals, http://www.oecd.org/chemicalsafety/testing/oecdguidelinesforthetestingofchemicals.htm (accessed 01/03/2017, 2017).
8 U. Liebel and W. Link, *Biotechnol. J.*, 2007, **2**, 938–940.
9 J. M. Zock, *Comb. Chem. High Throughput Screening*, 2009, **12**, 870–876.
10 D. J. Brayden, S.-A. Cryan, K. A. Dawson, P. J. O'Brien and J. C. Simpson, *Drug Discovery Today*, 2015, **20**, 942–957.
11 G. J. Ding, P. A. Fischer, R. C. Boltz, J. A. Schmidt, J. J. Colaianne, A. Gough, R. A. Rubin and D. K. Miller, *J. Biol. Chem.*, 1998, **273**, 28897–28905.
12 K. P. Sarker, H. Kataoka, A. Chan, S. J. Netherton, I. Pot, M. A. Huynh, X. Feng, A. Bonni, K. Riabowol and S. Bonni, *J. Biol. Chem.*, 2008, **283**, 13269–13279.
13 N. M. Radio, J. M. Breier, T. J. Shafer and W. R. Mundy, *Toxicol. Sci.*, 2008, **105**, 106–118.
14 B. Ruan, K. Pong, F. Jow, M. Bowlby, R. A. Crozier, D. Liu, S. Liang, Y. Chen, M. L. Mercado, X. Feng, F. Bennett, D. von Schack, L. McDonald, M. M. Zaleska, A. Wood, P. H. Reinhart, R. L. Magolda, J. Skotnicki, M. N. Pangalos, F. E. Koehn, G. T. Carter, M. Abou-Gharbia and E. I. Graziani, *Proc. Natl. Acad. Sci. U. S. A.*, 2008, **105**, 33–38.
15 S. Anguissola, D. Garry, A. Salvati, P. J. O'Brien and K. A. Dawson, *PLoS One*, 2014, **9**, e108025.
16 J. K. Morelli, M. Buehrle, F. Pognan, L. R. Barone, W. Fieles and P. J. Ciaccio, *Cell Biol. Toxicol.*, 2006, **22**, 15–27.
17 J. A. Dykens, J. D. Jamieson, L. D. Marroquin, S. Nadanaciva, J. J. Xu, M. C. Dunn, A. R. Smith and Y. Will, *Toxicol. Sci.*, 2008, **103**, 335–345.
18 F. Gasparri, M. Mariani, F. Sola and A. Galvani, *J. Biomol. Screening*, 2004, **9**, 232–243.
19 A. G. Walton, M. J. Deveney and J. L. Koenig, *Calcif. Tissue Res.*, 1970, **6**, 162–167.
20 G. Puppels and J. Greve, in *Biomedical Applications of Spectroscopy*, John Wiley and Sons, New York, 1996, vol. 25.
21 E. Efeoglu, A. Casey and H. J. Byrne, *Analyst*, 2016, **141**, 5417–5431.
22 E. Efeoglu, M. Keating, J. McIntyre, A. Casey and H. J. Byrne, *Anal. Methods*, 2015, **7**, 10000–10017.
23 Z. Farhane, F. Bonnier, M. A. Maher, J. Bryant, A. Casey and H. J. Byrne, *J. Biophotonics*, 2016, **10**, 151–165.

 This journal is © The Royal Society of Chemistry 2017

Published on 08 August 2017. Downloaded by Dublin Institute of Technology on 04/09/2017 12:27:54.

24 F. Bonnier, F. Petitjean, M. J. Baker and H. J. Byrne, *J. Biophotonics*, 2014, **7**, 167–179.
25 F. Bonnier, A. Mehmood, P. Knief, A. D. Meade, W. Hornebeck, H. Lambkin, K. Flynn, V. McDonagh, C. Healy, T. C. Lee, F. M. Lyng and H. J. Byrne, *J. Raman Spectrosc.*, 2011, **42**, 888–896.
26 J. Dorney, F. Bonnier, A. Garcia, A. Casey, G. Chambers and H. J. Byrne, *Analyst*, 2012, **137**, 1111–1119.
27 P. Knief, C. Clarke, E. Herzog, M. Davoren, F. M. Lyng, A. D. Meade and H. J. Byrne, *Analyst*, 2009, **134**, 1182–1191.
28 M. E. Keating, F. Bonnier and H. J. Byrne, *Analyst*, 2012, **137**, 5792–5802.
29 O. Lunov, T. Syrovets, C. Loos, G. U. Nienhaus, V. Mailander, K. Landfester, M. Rouis and T. Simmet, *ACS Nano*, 2011, **5**, 9648–9657.
30 O. Lunov, T. Syrovets, C. Loos, J. Beil, M. Delacher, K. Tron, G. U. Nienhaus, A. Musyanovych, V. Mailander, K. Landfester and T. Simmet, *ACS Nano*, 2011, **5**, 1657–1669.
31 T. Xia, M. Kovochich, M. Liong, J. I. Zink and A. E. Nel, *ACS Nano*, 2008, **2**, 85–96.
32 P. Ruenraroengsak and T. D. Tetley, *Part. Fibre Toxicol.*, 2015, **12**, 19.
33 F. Wang, L. Yu, M. P. Monopoli, P. Sandin, E. Mahon, A. Salvati and K. A. Dawson, *Nanomedicine*, 2013, **9**, 1159–1168.
34 M. G. Bexiga, J. A. Varela, F. Wang, F. Fenaroli, A. Salvati, I. Lynch, J. C. Simpson and K. A. Dawson, *Nanotoxicology*, 2011, **5**, 557–567.
35 M. Miljkovic, T. Chernenko, M. J. Romeo, B. Bird, C. Matthaus and M. Diem, *Analyst*, 2010, **135**, 2002–2013.
36 M. V. Berridge, P. M. Herst and A. S. Tan, *Biotechnol. Annu. Rev.*, 2005, **11**, 127–152.
37 S. N. Rampersad, *Sensors*, 2012, **12**, 12347–12360.
38 E. Vega-Avila and M. K. Pugsley, *Proc. West. Pharmacol. Soc.*, 2011, **54**, 10–14.
39 T. L. Riss, R. A. Moravec, A. L. Niles, S. Duellman, H. A. Benink, T. J. Worzella and L. Minor, in *Assay Guidance Manual*, ed. G. S. Sittampalam, N. P. Coussens, K. Brimacombe, A. Grossman, M. Arkin, D. Auld, C. Austin, B. Bejcek, M. Glicksman, J. Inglese, P. W. Iversen, Z. Li, J. McGee, O. McManus, L. Minor, A. Napper, J. M. Peltier, T. Riss, O. J. Trask Jr. and J. Weidner, Eli Lilly & Company and the National Center for Advancing Translational Sciences, Bethesda (MD), 2004.
40 J. O'Brien, I. Wilson, T. Orton and F. Pognan, *Eur. J. Biochem.*, 2000, **267**, 5421–5426.
41 T. Mosmann, *J. Immunol. Methods*, 1983, **65**, 55–63.
42 N. J. Marshall, C. J. Goodwin and S. J. Holt, *Growth Regul.*, 1995, **5**, 69–84.
43 R. Hamid, Y. Rotshteyn, L. Rabadi, R. Parikh and P. Bullock, *Toxicol. in Vitro*, 2004, **18**, 703–710.
44 T. Bernas and J. Dobrucki, *Cytometry*, 2002, **47**, 236–242.
45 M. A. Maher and H. J. Byrne, *Anal. Bioanal. Chem.*, 2016, **408**, 5295–5307.
46 V. Pliska, *J. Recept. Signal Transduction Res.*, 1999, **19**, 597–629.
47 Q. Mu, N. S. Hondow, L. Krzeminski, A. P. Brown, L. J. Jeuken and M. N. Routledge, *Part. Fibre Toxicol.*, 2012, **9**, 29.
48 K. Shapero, F. Fenaroli, I. Lynch, D. C. Cottell, A. Salvati and K. A. Dawson, *Mol. BioSyst.*, 2011, **7**, 371–378.
49 G.-Y. Liou and P. Storz, *Free Radical Res.*, 2010, **44**, 479–496.
50 J. F. Kerr, A. H. Wyllie and A. R. Currie, *Br. J. Cancer*, 1972, **26**, 239–257.
51 S. Elmore, *Toxicol. Pathol.*, 2007, **35**, 495–516.
52 L. Ouyang, Z. Shi, S. Zhao, F. T. Wang, T. T. Zhou, B. Liu and J. K. Bao, *Cell Proliferation*, 2012, **45**, 487–498.
53 G. Filomeni, D. De Zio and F. Cecconi, *Cell Death Differ.*, 2015, **22**, 377–388.
54 Z. Movasaghi, S. Rehman and I. U. Rehman, *Appl. Spectrosc. Rev.*, 2007, **42**, 493–541.
55 I. Notingher, S. Verrier, S. Haque, J. M. Polak and L. L. Hench, *Biopolymers*, 2003, **72**, 230–240.
56 I. Notingher and L. L. Hench, *Expert Rev. Med. Devices*, 2006, **3**, 215–234.
57 H. Abramczyk, B. Brozek-Pluska, M. Krzesniak, M. Kopec and A. Morawiec-Sztandera, *Spectrochim. Acta, Part A*, 2014, **129**, 609–623.
58 R. Vyumvuhore, A. Tfayli, H. Duplan, A. Delalleau, M. Manfait and A. Baillet-Guffroy, *Analyst*, 2013, **138**, 4103–4111.
59 E. Frohlich, C. Meindl, E. Roblegg, B. Ebner, M. Absenger and T. R. Pieber, *Part. Fibre Toxicol.*, 2012, **9**, 26.
60 B. M. Mohamed, N. K. Verma, A. M. Davies, A. McGowan, K. Crosbie-Staunton, A. Prina-Mello, D. Kelleher, C. H. Botting, C. P. Causey, P. R. Thompson, G. J. M. Pruijn, E. R. Kisin, A. V. Tkach, A. A. Shvedova and Y. Volkov, *Nanomedicine*, 2012, **7**, 1181–1195.
61 M. I. Sierra, A. Valdés, A. F. Fernández, R. Torrecillas and M. F. Fraga, *Int. J. Nanomed.*, 2016, **11**, 6297–6306.
62 S. R. Saptarshi, A. Duschl and A. L. Lopata, *J. Nanobiotechnol.*, 2013, **11**, 26.
63 E. C. Freeman, L. M. Weiland and W. S. Meng, *J. Biomater. Sci., Polym. Ed.*, 2013, **24**, 398–416.
64 R. V. Benjaminsen, M. A. Mattebjerg, J. R. Henriksen, S. M. Moghimi and T. L. Andresen, *Mol. Ther.*, 2013, **21**, 149–157.
65 M. A. Maher, P. C. Naha, S. P. Mukherjee and H. J. Byrne, *Toxicol. in Vitro*, 2014, **28**, 1449–1460.
66 H. Lullmann, R. Lullmann-Rauch and O. Wassermann, *Biochem. Pharmacol.*, 1978, **27**, 1103–1108.
67 N. D. Sonawane, J. R. Thiagarajah and A. S. Verkman, *J. Biol. Chem.*, 2002, **277**, 5506–5513.
68 L. Casteilla, M. Rigoulet and L. Pénicaud, *IUBMB Life*, 2001, **52**, 181–188.
69 S. P. Mukherjee and H. J. Byrne, *Nanomedicine*, 2013, **9**, 202–211.

Published on 08 August 2017. Downloaded by Dublin Institute of Technology on 04/09/2017 12:27:54.

70 R. J. DeBerardinis, *Genet. Med.*, 2008, **10**, 767–777.
71 T. D. Oberley and L. W. Oberley, *Histol. Histopathol.*, 1997, **12**, 525–535.
72 V. R. Jayanth, M. T. Bayne and M. E. Varnes, *Radiat. Res.*, 1994, **139**, 152–162.
73 S. Matsuyama and J. C. Reed, *Cell Death Differ.*, 2000, **7**, 1155–1165.
74 R. Halaby, *Res. Rep. Biol.*, 2015, **6**, 147–155.
75 O. LeGendre, P. A. Breslin and D. A. Foster, *Mol. Cell. Oncol.*, 2015, **2**, e1006077.
76 C. A. Owen, J. Selvakumaran, I. Notingher, G. Jell, L. L. Hench and M. M. Stevens, *J. Cell. Biochem.*, 2006, **99**, 178–186.
77 A. Bankapur, R. S. Krishnamurthy, E. Zachariah, C. Santhosh, B. Chougule, B. Praveen, M. Valiathan and D. Mathur, *PLoS One*, 2012, **7**, e35075.
78 K. Kong, C. Kendall, N. Stone and I. Notingher, *Adv. Drug Delivery Rev.*, 2015, **89**, 121–134.
79 I. Pence and A. Mahadevan-Jansen, *Chem. Soc. Rev.*, 2016, **45**, 1958–1979.
80 M. E. Keating and H. J. Byrne, *Nanomedicine*, 2013, **8**, 1335–1351.
81 A. Ettinger and T. Wittmann, *Methods Cell Biol.*, 2014, **123**, 77–94.
82 D. A. Basiji, W. E. Ortyn, L. Liang, V. Venkatachalam and P. Morrissey, *Clin. Lab. Med.*, 2007, **27**, 653–670.

This journal is © The Royal Society of Chemistry 2017